ACS APPLIED MATERIALS & INTERFACES

Research Article

www.acsami.org

Excellent Electromagnetic Absorption Properties of Poly(3,4-ethylenedioxythiophene)-Reduced Graphene Oxide–Co_3O_4 Composites Prepared by a Hydrothermal Method

Pan-Bo Liu, Ying Huang,* and Xu Sun

Key Laboratory of Space Applied Physics and Chemistry, Ministry of Education, School of Science, Northwestern Polytechnical University, Xi'an 710129, PR China

ABSTRACT: The ternary composites of poly(3,4-ethylenedioxythiophene)-reduced graphene oxide–Co_3O_4 (PEDOT–RGO–Co_3O_4) were synthesized and the electromagnetic absorption property of the composites was investigated. The structure of the composites was characterized with Fourier-transform infrared spectra, X-ray diffraction, Raman spectroscopy, X-ray photoelectron spectroscopy, and transmission electron microscope. The electromagnetic parameters indicate the enhanced electromagnetic absorption property of the composites was attributed to the better impedance matching. On the basis of the above characterization, an electromagnetic complementary theory was proposed to explain the impedance matching. It can be found that the maximum reflection loss of PEDOT–RGO–Co_3O_4 can reach −51.1 dB at 10.7 GHz, and the bandwidth exceeding −10 dB is 3.1 GHz with absorber thickness of 2.0 mm. Therefore, the PEDOT–RGO–Co_3O_4 composites, with such excellent electromagnetic absorption properties and wide absorption bandwidth, can be used as a new kind of candidate for microwave absorbing materials.

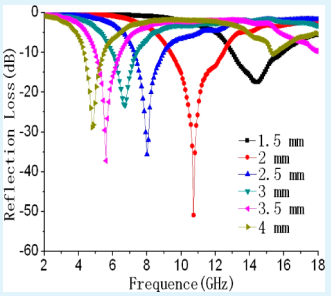

KEYWORDS: *graphene, conducting polymers, magnetic nanoparticles, electromagnetic parameters, microwave absorbing materials*

1. INTRODUCTION

Microwave absorbing materials can absorb electromagnetic waves and convert electromagnetic energy into other types of energy or make the electromagnetic wave dissipate.[1] According to the electromagnetic energy conversion principle, the following three factors affect the electromagnetic absorption property: dielectric loss, magnetic loss, and impedance matching characteristics.[2,3] However, most of electromagnetic wave absorbers are composed of dielectric or magnetic materials,[4−6] and their impedance matching characteristics have seldom been studied.

Reduced graphene oxide (RGO) has attracted much attention in the science world during recent years due to its unique properties.[7−10] High dielectric loss and low density enable it to be used as a microwave absorbing material. However, RGO is found to be nonmagnetic and its electromagnetic absorption properties mostly contribute to dielectric loss; therefore, it is not an ideal microwave absorbing material.[11] On the basis of the electromagnetic complementary theory, one of the effective ways to solve the problem is to couple RGO with magnetic particles. In recently, magnetic particles have attracted considerable attentions due to their controllable size and shape, and the electromagnetic absorption property can be determined by their properties.[12,13] Previous reports demonstrated that the electromagnetic absorption property of RGO can be enhanced by adding Fe_3O_4 particles.[14−16] However, the shortage of Fe_3O_4 particles hampers their applications. As an important semiconducting transition metal oxide, Co_3O_4 is considered to be a most promising material due to its special properties and controllable structure.[17−20] Furthermore, Co_3O_4 composites have been investigated extensively in recent years in many fields, such as batteries,[21−23] supercapacitors,[24−27] and microwave absorption materials.[28,29]

Poly(3,4-ethylenedioxythiophene) (PEDOT), the conducting polymer, can be used as a microwave absorbing material due to its high electrical conductivity.[30] Therefore, the composites containing PEDOT can be used as microwave absorbing materials.[31] Recently, the novel ternary composites of expanded graphite/polyaniline/$CoFe_2O_4$ (EG/PANI/CF) ferrite have been synthesized,[32] but the maximum reflection loss of the composites is −19.13 dB with a thickness of 0.5 mm. Singh has developed a 3D nanoarchitecture in polyaniline by incorporating a hybrid structure of graphene/Fe_3O_4. However, the electromagnetic interference shielding effectiveness is only 26 dB.[33] Liu has covered RGO with PEDOT aggregations and studied the microwave absorption properties of the composites composed of RGO–PEDOT and Co_3O_4 particles, but the absorption bandwidth exceeding −10 dB is very narrow (only 2.1 GHz).[34]

In order to reduce or remove the PEDOT aggregations, we use ethanol as a dispersant to facilitate the diffusion of 3,4-ethylenedioxythiophene monomer, because it plays an irreplaceable role in the uniform coating process of PEDOT. It is confirmed that RGO can be completely covered by PEDOT and subsequently the incorporation of Co_3O_4 particles effectively improves the electromagnetic absorption properties and widens the absorption bandwidth. It is imperative to

Received: July 23, 2013
Accepted: November 12, 2013
Published: November 12, 2013

investigate the relationship of the electromagnetic parameters between PEDOT, RGO, and Co_3O_4 particles. The results indicate that the electromagnetic attenuation mechanism of PEDOT−RGO−Co_3O_4 is attributed to better impedance matching. The maximum reflection loss of the composites is −51.1 dB at 10.7 GHz and the bandwidth below −10 dB is 3.1 GHz (from 9.4 to 12.5 GHz) with a thickness of 2.0 mm, thus the electromagnetic absorption property and the absorption bandwidth of the composites are better than the previous report.[34]

2. EXPERIMENTAL SECTION

Preparation. Graphene oxide (GO) was synthesized via a modified Hummer method.[35] PEDOT−RGO−Co_3O_4 was prepared as follows: 3,4-ethylenedioxythiophene monomer (0.4 mL) dispersed in ethanol (30 mL) was added into GO (100 mL, 1 mg/mL) solution by sonication treatment, then the solutioon was cooled down to 0 °C. The concentrated H_2SO_4 (2 mL) and $(NH_4)_2S_2O_8$ (0.95 g) dissolved in distilled water (10 mL) were added into the above solution orderly and the mixture stirred constantly at this temperature for 12 h. The precipitate was washed with distilled water several times. The synthetic procedure of PEDOT−RGO−Co_3O_4 was according to our previous work.[36] To show the difference, PEDOT−RGO was synthesized under a similar method without adding $CoCl_2{\cdot}6H_2O$. RGO was prepared via the chemical reduction of GO with hydrazine hydrate.

Characterization. Fourier transform infrared (FTIR) spectra were recorded on a NICOLET iS10. The crystal structure was characterized on X-ray diffraction (D/max 2550 V, Cu Kα radiation). The morphology and size of the composites were characterized by field emission transmission electron microscope (FETEM: Tecnai F30 G^2). Raman spectroscopy was carried out on a Renishaw in Via Raman Microscope. The chemical states were investigated by X-ray photoelectron spectroscopy (XPS, PHI 5300X). The electromagnetic parameters were measured in a HP8753D vector network analyzer. The samples were prepared by mixing the composites and paraffin wax at 50% weight fraction of each. The samples were pressed into a toroidal shape (φ_{out} 7.0 mm; φ_{in} 3.0 mm).

3. EXPERIMENTAL RESULTS AND THEIR DISCUSSION

Figure 1 shows that the peaks at about 1513 and 1342 cm^{-1} in the literature are ascribed to the C═C/C—C stretching of the

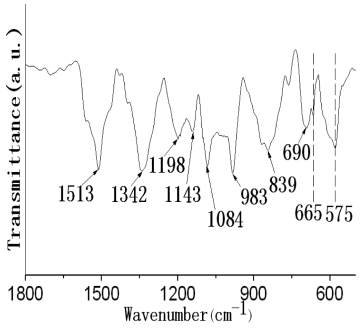

Figure 1. FT-IR spectra of PEDOT−RGO−Co_3O_4 composites.

thiophene rings, and the peaks at 1198, 1143, and 1084 cm^{-1} in the literature are attributed to the C—O—C stretching, respectively. Moreover, the peaks at 983 and 839 cm^{-1} are ascribed to the oxyethylene ring stretching and the peak at 690 cm^{-1} is attributed to the symmetric C—S—C stretching in the thiophene ring, respectively.[37,38] The series of these peaks in above-mentioned indicate that PEDOT is successfully grown onto RGO. In addition, two other peaks at 575 and 665 cm^{-1} are attributed to the Co—O stretching, suggesting the presence of Co_3O_4 particles in the composites.[39]

XRD is employed to investigate the structure of the samples and the corresponding results are presented in Figure 2. For

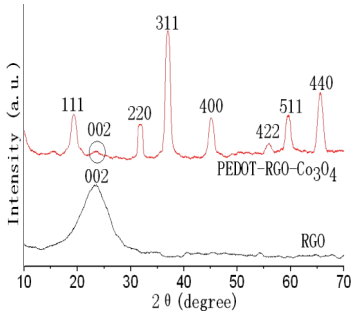

Figure 2. XRD patterns of RGO and PEDOT−RGO−Co_3O_4 composites.

RGO, the characteristic diffraction peak at around 24.9° can be due to the graphitic structure (002) of short-range order in stacked RGO.[40] For PEDOT−RGO−Co_3O_4, the seven peaks centered at 19.2°, 31.8°, 36.9°, 45.0°, 55.8°, 59.6°, and 65.5° match well with the standard XRD data for the (111), (220), (311), (400), (422), (511), and (440) planes of Co_3O_4 (JCPDS no. 43-1003). Furthermore, the weak intensity peaks indicate that the size of Co_3O_4 particles is small. In addition, a small and weak diffraction peak centered at about 25.1° can be attributed to the disorderedly stacked RGO.[23] No other peaks can be observed, indicating the high purity of PEDOT−RGO−Co_3O_4.

In Figure 3, the Raman spectrum of RGO is associated with a typical D band at 1347 cm^{-1} and a G band at 1581 cm^{-1}. The

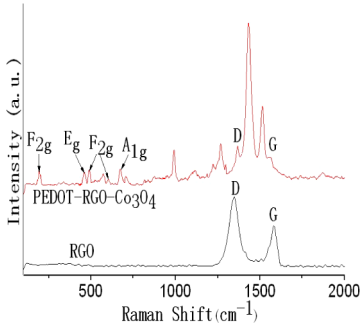

Figure 3. Raman spectroscopy of RGO and PEDOT−RGO−Co_3O_4 composites.

D band is due to the breathing mode of κ-point photons of A_{1g} symmetry and the G band arises from the first-order scattering of E_{2g} phonons by sp^2 carbon atoms.[41,42] For PEDOT−RGO−Co_3O_4 composites, apart from the D and G bands, the typical Raman spectrum of PEDOT also can be observed in PEDOT−RGO−Co_3O_4 composites. The peak at 698 cm^{-1} is attributed to symmetric C—S—C deformation, the peak at 986 cm^{-1} is attributed to oxyethylene ring deformation and the peaks at 1431 and 1518 cm^{-1} are attributed to C═C stretching.[43,44] The D and G bands in PEDOT−RGO−Co_3O_4 composites exhibit a red shift compared with that of RGO, the respective red shift would be due to the strong interaction between PEDOT and RGO. Furthermore, the Raman peaks centered at 190, 489, and 602 cm^{-1} are attributed to the F_{2g} modes of

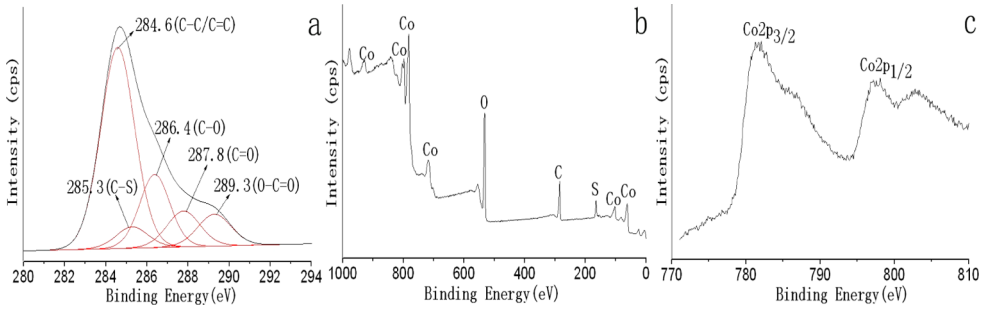

Figure 4. C 1s (a), wide scan (b) and Co 2p (c) XPS spectra of PEDOT−RGO−Co_3O_4 composites.

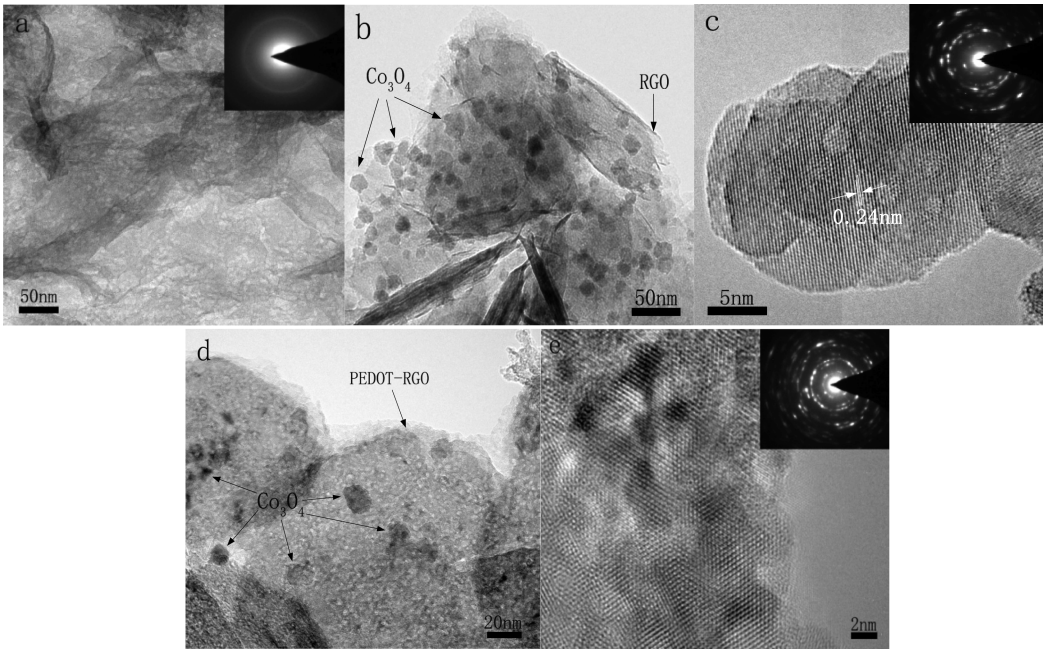

Figure 5. TEM images of PEDOT−RGO (a), RGO−Co_3O_4 (b), and PEDOT−RGO−Co_3O_4 (d). HRTEM images of RGO−Co_3O_4 (c) and PEDOT−RGO−Co_3O_4 composites (e).

Co_3O_4, and the peaks at 460 and 670 cm^{-1} are attributed to the E_g and A_{1g} modes of Co_3O_4, respectively.[45] All of the above analyses confirm the successful formation of PEDOT−RGO−Co_3O_4 composites.

The chemical state of the elements in PEDOT−RGO−Co_3O_4 composites is further investigated with XPS in Figure 4. Figure 4a shows that the C1s XPS spectra of PEDOT−RGO−Co_3O_4 composites deconvoluted into five different peaks. The peaks centered at 284.6, 286.4, 287.8, and 289.3 eV can be attributed to the C—C/C═C, C—O, or alkoxy, C═O and O—C═O groups, respectively.[46] In addition, the new peak centered at 285.3 eV is due to the C−S group.[47,48] In Figure 4b, the wide scan XPS spectrum indicates that the existence of C, O, S, and Co elements in the composites. In Figure 4c, the Co 2p XPS spectra of the composites exhibit two binding energy peaks at 781.3 and 797.4 eV, corresponding to Co $2p_{3/2}$ and Co $2p_{1/2}$, respectively.[49,50] From the above analysis, we can deduce that the presence of Co_3O_4 particles in the composites and the results are consistent with the Raman spectroscopy.

The microstructure of the composites is analyzed with TEM, and the results are presented in Figure 5. Figure 5a reveals that PEDOT−RGO composites have many wrinkled forms and no PEDOT aggregations can be observed, indicating that PEDOT is uniformly covered on the surface of RGO, which is different from the previous work.[34] The SAED patterns at this region (inset in Figure 5a) indicate that PEDOT−RGO lack crystalline characteristics, showing that RGO is completely covered with PEDOT. Figure 5b, giving the TEM image of RGO−Co_3O_4, shows that many small Co_3O_4 particles, with the average diameter between 10 and 20 nm, are uniformly anchored onto RGO (indicated by the arrows). Besides, these Co_3O_4 particles are firmly attached onto RGO that even sonication is used during the preparation of TEM specimens, indicating an excellent adhesion between Co_3O_4 particles and RGO is formed. Figure 5c is the corresponding HRTEM image. The well-defined lattice planes of Co_3O_4 particles can be observed and the crystal lattice spacing (0.24 nm) can be attributed to the (311) plane of Co_3O_4 particles, which is consistent with the result of XRD. The SAED patterns (inset in Figure 5c) obtained from a typical individual particle also demonstrates the crystalline feature of Co_3O_4 particles. Figure 5d shows that many Co_3O_4 particles covered on the wrinkled surface of PEDOT−RGO (indicated by the arrows). In order to verify the crystalline structure of Co_3O_4 particles, HRTEM image of PEDOT−RGO−Co_3O_4 composites is presented in Figure 5e. The HRTEM image and SAED patterns (inset in Figure 5e) clearly demonstrate the crystalline nature of Co_3O_4 particles.

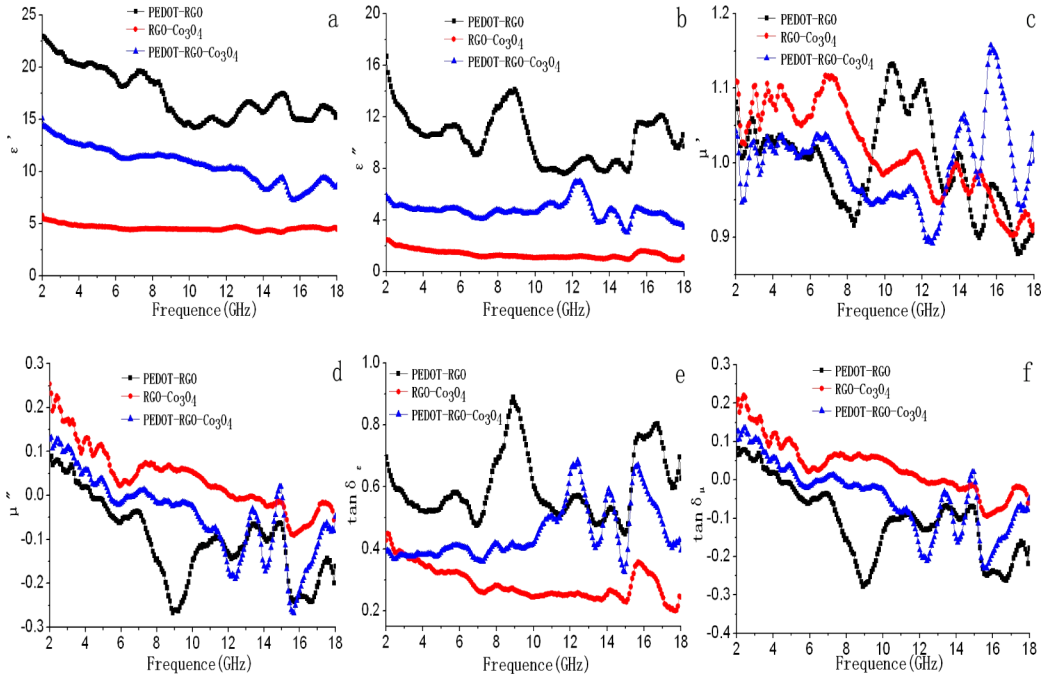

Figure 6. Values of ε' (a), ε'' (b), μ' (c), μ'' (d), tan $\delta\varepsilon$ (e), and tan $\delta\mu$ (f) for PEDOT−RGO, RGO−Co_3O_4, and PEDOT−RGO−Co_3O_4 composites.

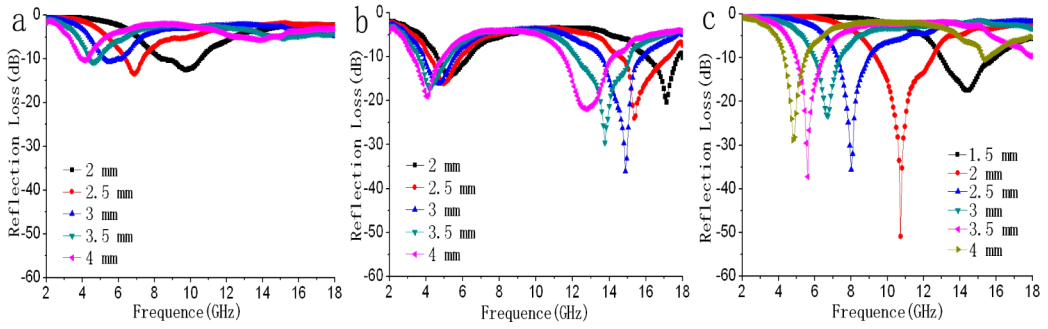

Figure 7. Reflection loss curves of PEDOT−RGO (a), RGO−Co_3O_4 (b), and PEDOT−RGO−Co_3O_4 composites (c).

The permittivity real part (ε'), permittivity imaginary part (ε''), permeability real part (μ'), permeability imaginary part (μ''), dielectric loss tangent (tan $\delta\varepsilon$), and magnetic loss tangent (tan $\delta\mu$) of the composites are presented in Figure 6. Figure 6a shows that the ε' values of PEDOT−RGO and PEDOT−RGO−Co_3O_4 decrease gradually from 23.1 to 15.6 and 15.1 to 8.7, respectively, with some fluctuations over 2−18 GHz frequency range, and their ε'' values (Figure 6b) vary from 16.7 to 7.7 and 7.1 to 3.1, respectively, with the variation in the frequency range of 2−18 GHz. For RGO−Co_3O_4, the values of ε' (Figure 6a) and ε'' (Figure 6b) negligibly decline from 5.6 to 4.5 and 2.5 to 1.1, respectively. Moreover, the above figures show that PEDOT−RGO exhibits higher ε' and ε'' values than RGO−Co_3O_4 and PEDOT−RGO−Co_3O_4 composites; this phenomenon may be due to the conducting polymers of PEDOT covered onto RGO. In Figure 6c and d, the μ' and μ'' values of the above three composites exhibit complex fluctuations in the frequency range of 2−18 GHz. With the introduction of Co_3O_4 particles, there is sign of a magnetic ascension which is noticeable from the enhanced permeability. It also can be seen that the μ'' values of the composites are negative at high frequency, especially for PEDOT−RGO, indicating that magnetic energy is radiated out from the composites. Figure 6e and f shows that tan $\delta\varepsilon$ values of PEDOT−RGO are higher than those of RGO−Co_3O_4 and PEDOT−RGO−Co_3O_4, while tan $\delta\mu$ values are lower than the other two. The results suggest the electromagnetic attenuation mechanism of PEDOT−RGO is mainly attributed to dielectric loss. As mentioned in the previous report,[51] the electromagnetic absorption property of absorbers also dependents on the combination between magnetic loss and dielectric loss. The dielectric loss and magnetic loss of PEDOT−RGO are out of balance,[52] thus the absorption of PEDOT−RGO is weak. Because Co_3O_4 particles have magnetic characteristics, the PEDOT−RGO−Co_3O_4 composites consisting of RGO, PEDOT, and Co_3O_4 particles may have better impedance matching, thus the PEDOT−RGO−Co_3O_4 composites will have an excellent electromagnetic absorption property. First, dipole polarization is presented in Co_3O_4 particles with nanoscale size. The small size of Co_3O_4 particle increases the dipole polarization, thus contributing to dielectric loss.[53,54] Second, the dielectric loss is related to the natural structure of Co_3O_4. Electronic polarization and ion polarization may take place during the electron transfer process between cobalt ions, which also has effect on the electromagnetic absorption property. Third, at the interface of the ternary composites,

dx.doi.org/10.1021/am404561c | ACS Appl. Mater. Interfaces 2013, 5, 12355−12360

interface defects can function as polarized centers, leading to an additional dielectric loss.[55] In addition, the better matching impedance also plays an important role in increasing the electromagnetic absorption property. From the above analyses, we can draw a conclusion that the electromagnetic absorption property of PEDOT−RGO−Co_3O_4 composites can be attributed to the efficient complementarities.

The reflection loss (R_L) values of the composites are calculated according to the following equations.[56]

$$R_L(\mathrm{dB}) = 20\log\left|\frac{Z_{in} - 1}{Z_{in} + 1}\right| \quad (1)$$

$$Z_{in} = \sqrt{\mu_r/\varepsilon_r}\,\tanh\left[j(2\pi fd/c)\sqrt{\varepsilon_r\mu_r}\right] \quad (2)$$

Where Z_{in} is the input impedance of the absorber, f is the frequency of electromagnetic waves, d is the thickness of the absorber, and c is the velocity of electromagnetic waves in free space. Figure 7a shows that PEDOT−RGO exhibits poor microwave absorption properties. The maximum R_L is −13.4 dB at 6.9 GHz when its thickness is 2.5 mm. Figure 7b shows that RGO−Co_3O_4 has a strong reflection loss peak and a maximum R_L of −36.1 dB at 14.9 GHz with a thickness of 3 mm, and the absorption bandwidth exceeding −10 dB is 3.7 GHz. Furthermore, the maximum R_L values shift to a lower frequency range when the layer thickness increases. Compared with the above two composites, PEDOT−RGO−Co_3O_4 composites exhibit excellent microwave absorption properties as shown in Figure 7c. It can be found that the maximum R_L is down to −51.1 dB at 10.7 GHz and the absorption bandwidth exceeding −10 dB is 3.1 GHz (from 9.4 to 12.5 GHz) with absorber thicknesses of 2.0 mm. The microwave absorption properties of the composites are better than the two-component composites, such as RGO−Fe_3O_4 nanoparticles,[14,15,57,58] RGO−Ni nanocrystals,[59] RGO−$NiFe_2O_4$ nanoparticles,[60] Fe_3O_4−barium ferrite,[61] Fe_3O_4−PEDOT,[31] and the ternary composites of expanded graphite/polyaniline/$CoFe_2O_4$[32] and polyaniline/graphene/Fe_3O_4.[33] The introduction of Co_3O_4 particles improves the impedance matching, which helps to enhance the electromagnetic absorption property of PEDOT−RGO.

4. CONCLUSIONS

In summary, we present the simple hydrothermal method to prepare ternary composites consisting of PEDOT, RGO, and Co_3O_4 particles. The results indicate that RGO is uniformly covered by PEDOT due to the present of ethanol, and Co_3O_4 particles with average diameter within the range of 10−30 nm are also firmly anchored onto PEDOT−RGO. The electromagnetic absorption property of PEDOT−RGO is mainly attributed to dielectric loss, but the electromagnetic attenuation mechanism of PEDOT−RGO−Co_3O_4 composites is attributed to the better impedance matching. Comparing with PEDOT−RGO and RGO−Co_3O_4, PEDOT−RGO−Co_3O_4 composites exhibit excellent electromagnetic absorption property. The maximum R_L is up to −51.1 dB at 10.7 GHz and the bandwidth exceeding −10 D is 3.1 GHz when the thickness is 2.0 mm. The results indicate that the combination of RGO with PEDOT and Co_3O_4 particles enables the novel hybrid materials to be used as lightweight and high-efficiency electromagnetic wave absorption materials.

AUTHOR INFORMATION

Corresponding Author

*E-mail: yingh@nwpu.edu.cn. Tel.: + 86 029-88431636.

Notes

The authors declare no competing financial interest.

ACKNOWLEDGMENTS

Research was supported by the Spaceflight Foundation of the People's Republic of China (NBXW0001), the Spaceflight Innovation Foundation of China (NBXT0002), and the Doctorate Foundation of Northwestern Polytechnical University (CX201328).

REFERENCES

(1) Liu, J. W.; Che, R. C.; Chen, H. J.; Zhang, F.; Xia, F.; Wu, Q. S.; Wang, M. *Small* **2012**, *8*, 1214−1221.
(2) Xu, P.; Han, X. J.; Wang, C.; Zhou, D. H.; Lv, Z. S.; Wen, A. H.; Wang, X. H.; Zhang, B. *J. Phys. Chem. B* **2008**, *112*, 10443−10449.
(3) Yan, L. G.; Wang, J. B.; Han, X. H.; Ren, Y.; Liu, Q. F.; Li, F. S. *Nanotechnology* **2010**, *21*, 095708.
(4) Zhu, W. M.; Wang, L.; Zhao, R.; Ren, J. W.; Lu, G. Z.; Wang, Y. Q. *Nanoscale* **2011**, *3*, 2862−2864.
(5) Wang, C.; Han, X. J.; Zhang, X. L.; Hu, S. R.; Zhang, T.; Wang, J. Y.; Du, Y. C.; Wang, X. H.; Xu, P. *J. Phys. Chem. C* **2010**, *114*, 14826−14830.
(6) Deng, L. J.; Han, M. G. *Appl. Phys. Lett.* **2007**, *91*, 023119.
(7) Novoselov, K. S.; Geim, A. K.; Morozov, S. V.; Jiang, D.; Zhang, Y.; Dubonos, S. V.; Grigorieva, I. V.; Firsov, A. A. *Science* **2004**, *306*, 666−669.
(8) Dikin, D. A.; Tankovich, S. S.; Zimney, E. J.; Piner, R. D.; Dommett, G. H. B.; Evmenenko, G.; Nguyen, S. T.; Ruoff, R. S. *Nature* **2007**, *448*, 457−460.
(9) Zhu, Y. W.; Murali, S.; Cai, W. W.; Li, X. S.; Suk, J. W.; Potts, J. R.; Ruoff, R. S. *Adv. Mater.* **2010**, *22*, 3906−3924.
(10) Park, S.; Suk, J. W.; An, J.; Oh, J.; Lee, S.; Lee, W.; Potts, J. R.; Byun, J. H.; Ruoff, R. S. *Carbon* **2012**, *50*, 4573−4578.
(11) Wang, C.; Han, X. J.; Xu, P.; Zhang, X. L.; Du, Y. C.; Hu, S. R.; Wang, J. Y.; Wang, X. H. *Appl. Phys. Lett.* **2011**, *98*, 072906.
(12) Sun, G. B.; Dong, B. X.; Cao, M. H.; Wei, B. Q.; Hu, C. W. *Chem. Mater.* **2011**, *23*, 1587−1593.
(13) Tong, G. X.; Hu, Q.; Wu, W. H.; Li, W.; Qian, H. S.; Liang, Y. *J. Mater. Chem.* **2012**, *22*, 17494−17504.
(14) Xu, H. L.; Bi, H.; Yang, R. B. *J. Appl. Phys.* **2012**, *111*, 07A522.
(15) Sun, X.; He, J. P.; Li, G. X.; Tang, J.; Wang, T.; Guo, Y. X.; Xue, H. R. *J. Mater. Chem. C* **2013**, *1*, 765−777.
(16) Ren, Y. L.; Wu, H. Y.; Lu, M. M.; Chen, Y. J.; Zhu, C. L.; Gao, P.; Cao, M. S.; Li, C. Y.; Ouyang, Q. Y. *ACS Appl. Mater. Interfaces* **2012**, *4*, 6436−6442.
(17) Wei, T. Y.; Chen, C. H.; Chang, K. H.; Lu, S. Y.; Hu, C. C. *Chem. Mater.* **2009**, *21*, 3228−3233.
(18) Zhu, T.; Chen, J. S.; Lou, X. W. *J. Mater. Chem.* **2010**, *20*, 7015−7020.
(19) Mei, W. M.; Huang, J.; Zhu, L. P.; Ye, Z. Z.; Maia, Y. J.; Tua, J. P. *J. Mater. Chem.* **2012**, *22*, 9315−9321.
(20) Wang, H. T.; Zhang, L.; Tan, X. H.; Holt, C. M. B.; Zahiri, B.; Olsen, B. C.; Mitlin, D. *J. Phys. Chem. C* **2011**, *115*, 17599−17605.
(21) Lou, X. W.; Deng, D.; Lee, J. Y.; Feng, J.; Archer, L. A. *Adv. Mater.* **2008**, *20*, 258−262.
(22) Kim, H.; Seo, D. H.; Kim, S. W.; Kim, J.; Kang, K. *Carbon* **2011**, *49*, 326−332.
(23) Wu, Z. S.; Ren, W. C.; Wen, L.; Gao, L. B.; Zhao, J. P.; Chen, Z. P.; Zhou, G. M.; Li, F.; Cheng, H. M. *ACS Nano* **2010**, *4*, 3187−3194.
(24) Wang, B.; Zhu, T.; Wu, H. B.; Xu, R.; Chen, J. S.; Lou, X. W. *Nanoscale* **2012**, *4*, 2145−2149.
(25) Zhou, W. W.; Liu, J. P.; Chen, T.; Tan, K. S.; Jia, X. T.; Luo, Z. Q.; Cong, C. X.; Yang, H. P.; Li, C. M.; Yu, T. *Phys. Chem. Chem. Phys.* **2011**, *13*, 14462−14465.

(26) Xia, X. H.; Tu, J. P.; Wang, X. L.; Gu, C. D.; Zhao, X. B. *Chem. Commun.* **2011**, *47*, 5786−5788.
(27) Meher, S. K.; Rao, G. R. *J. Phys. Chem. C* **2011**, *115*, 15646−15654.
(28) Liu, P. B.; Huang, Y.; Wang, L.; Zong, M.; Zhang, W. *Mater. Lett.* **2013**, *107*, 166−169.
(29) Liu, P. B.; Huang, Y.; Wang, L. *J. Alloys Compd.* **2013**, *573*, 151−156.
(30) Ni, X. W.; Hu, X. J.; Zhou, S. Y.; Sun, C. H.; Bai, X. X.; Chen, P. *Polym. Adv. Technol.* **2011**, *22*, 532−537.
(31) Zhou, W. C.; Hu, X. J.; Bai, X. X.; Zhou, S. Y.; Sun, C. H.; Yan, J.; Chen, P. *ACS Appl. Mater. Interfaces* **2011**, *3*, 3839−3845.
(32) Chen, K. Y.; Xiang, C.; Li, L. C.; Qian, H. S.; Xiao, Q. S.; Xu, F. *J. Mater. Chem.* **2012**, *22*, 6449−6455.
(33) Singh, K.; Ohlan, A.; Pham, V. H.; Balasubramaniyan, R.; Varshney, S.; Jang, J.; Hur, S. H.; Choi, W. M.; Kumar, M.; Dhawan, S. K.; Kong, B. S.; Chung, J. S. *Nanoscale* **2013**, *5*, 2411−2420.
(34) Liu, P. B.; Huang, Y. *RSC Adv.* **2013**, *3*, 19033−19039.
(35) Hummers, W. S.; Offeman, R. E. *J. Am. Chem. Soc.* **1958**, *80*, 1339−1339.
(36) Liu, P. B.; Huang, Y.; Wang, L.; Zhang, W. *J. Alloys Compd.* **2013**, *573*, 151−156.
(37) Xu, Y. F.; Wang, Y.; Liang, J. J.; Huang, Y.; Ma, Y. F.; Wan, X. J.; Chen, Y. S. *Nano Res.* **2009**, *2*, 343−348.
(38) Alvi, F.; Ram, M. K.; Basnayakab, P. A.; Stefanakosa, E.; Goswamid, Y.; Kumarb, A. *Electrochim. Acta* **2011**, *56*, 9406−9412.
(39) Xia, X. H.; Tu, J. P.; Mai, Y. J.; Wang, X. L.; Gu, C. D.; Zhao, X. B. *J. Mater. Chem.* **2011**, *21*, 9319−9325.
(40) Si, Y. C.; Samulski, E. T. *Chem. Mater.* **2008**, *20*, 6792−6797.
(41) Jin, Z.; Yao, J.; Kittrell, C.; Tour, J. M. *ACS Nano* **2011**, *5*, 4112−4117.
(42) Chen, W. F.; Li, S. R.; Chen, C. H.; Yan, L. F. *Adv. Mater.* **2011**, *23*, 5679−5683.
(43) Zhang, J. T.; Zhao, X. S. *J. Phys. Chem. C* **2012**, *116*, 5420−5426.
(44) Schaarschmidt, A.; Farah, A. A.; Aby, A.; Helmy, A. S. *J. Phys. Chem. B* **2009**, *113*, 9352−9355.
(45) Li, B. J.; Cao, H. Q.; Shao, J.; Li, G. Q.; Qu, M. Z.; Gui, Y. *Inorg. Chem.* **2011**, *50*, 1628−1632.
(46) Shin, H. J.; Kim, K. K.; Benayad, A.; Yoon, S. M.; Park, H. K.; Jung, I. S.; Jin, M. H.; Jeong, H. K.; Kim, J. M.; Choi, J. Y.; Lee, Y. H. *Adv. Funct. Mater.* **2009**, *19*, 1987−1992.
(47) Spanninga, S. A.; Martin, D. C.; Chen, Z. *J. Phys. Chem. C* **2009**, *113*, 5585−5592.
(48) Spanninga, S. A.; Martin, D. C.; Chen, Z. *J. Phys. Chem. C* **2010**, *114*, 14992−14997.
(49) Yuan, C. Z.; Yang, L.; Hou, L. R.; Li, J. Y.; Sun, Y. X.; Zhang, X. G.; Shen, L. F.; Lu, X. J.; Xiong, S. L.; Lou, X. W. *Adv. Funct. Mater.* **2012**, *22*, 2560−2566.
(50) Liang, Y. Y.; Li, Y. G.; Wang, H. L.; Zhou, J. G.; Wang, J.; Regier, T.; Dai, H. J. *Nat. Mater.* **2011**, *10*, 780−786.
(51) Chen, Y. J.; Gao, P.; Zhu, C. L.; Wang, R. X.; Wang, L. J.; Cao, M. S.; Fang, X. Y. *J. Appl. Phys.* **2009**, *106*, 054303.
(52) Zhou, J. H.; He, J. P.; Li, G. X.; Wang, T.; Sun, D.; Ding, X. C.; Zhao, J. Q.; Wu, S. C. *J. Phys. Chem. C* **2010**, *114*, 7611−7617.
(53) Chen, Y. J.; Cao, M. S.; Wang, T. H.; Wan, Q. *Appl. Phys. Lett.* **2004**, *84*, 3367.
(54) Chen, Y. J.; Zhang, F.; Zhao, G. G.; Fang, X. Y.; Jin, H. B.; Gao, P.; Zhu, C. L.; Cao, M. S.; Xiao, G. *J. Phys. Chem. C* **2010**, *114*, 9239−9244.
(55) Lagarkov, A. K.; Sarychev, A. K. *Phys. Rev. B* **1996**, *53*, 6318−6336.
(56) Kim, S. S.; Jo, S. B.; Choi, K. K.; Kim, J. M.; Churn, K. S. *IEEE Trans. Magn.* **1991**, *27*, 5462−5464.
(57) Li, X. H.; Yi, H. B.; Zhang, J. W.; Feng, J.; Li, F. S.; Xue, D. S.; Zhang, H. L.; Peng, Y.; Mellors, N. J. *J. Nanopart. Res.* **2013**, *15*, 1472.
(58) Ma, E. L.; Li, J. J.; Zhao, N. Q.; Liu, E. Z.; He, C. N.; Shi, C. S. *Mater. Lett.* **2013**, *91*, 209−212.
(59) Chen, T.; Deng, F.; Zhu, J.; Chen, C.; Sun, G.; Ma, S.; Yang, X. *J. Mater. Chem.* **2012**, *22*, 15190−15197.
(60) Fu, M.; Jiao, Q. Z.; Zhao, Y. *J. Mater. Chem. A* **2013**, *1*, 5577−5586.
(61) Ohlan, A.; Singh, K.; Amita Chandra, A.; Dhawan, S. K. *ACS Appl. Mater. Interfaces* **2010**, *2*, 927−933.